Обзор ArXiv: astro-ph, 2-5 мая 2017 года

От Сильченко О.К.

Astro-ph: 1705.00425

Torus Models of the Outer Disc of the Milky Way using LAMOST Survey Data

Qiao Wang[1⋆], Yougang Wang[1], Chao Liu[2], Shude Mao[3,1,4], R. J. Long[5,4]
[1] *Key Laboratory of Computational Astrophysics, National Astronomical Observatories, Chinese Academy of Sciences, Beijing, 100012 China*
[2] *Key Laboratory of Optical Astronomy, National Astronomical Observatories, Chinese Academy of Sciences, Beijing, 100012 China*
[3] *Department of Physics, and Center for Astrophysics, Tsinghua University, 100086 Beijing, China*
[4] *Jodrell Bank Centre for Astrophysics, School of Physics and Astronomy, The University of Manchester, Oxford Road, Manchester M13 9PL, UK*
[5] *National Astronomical Observatories, Chinese Academy of Sciences, Beijing, 100012 China*

Accepted XXX. Received YYY; in original form ZZZ

ABSTRACT
With a sample of 48,161 K giant stars selected from the LAMOST DR 2 catalogue, we construct torus models in a large volume extending, for the first time, from the solar vicinity to a Galactocentric distance of ~ 20 kpc, reaching the outskirts of the Galactic disc. We show that the kinematics of the K giant stars match conventional models, e.g. as created by Binney in 2012, in the Solar vicinity. However such two-disc models fail if they are extended to the outer regions, even if an additional disc component is

Исследованные области

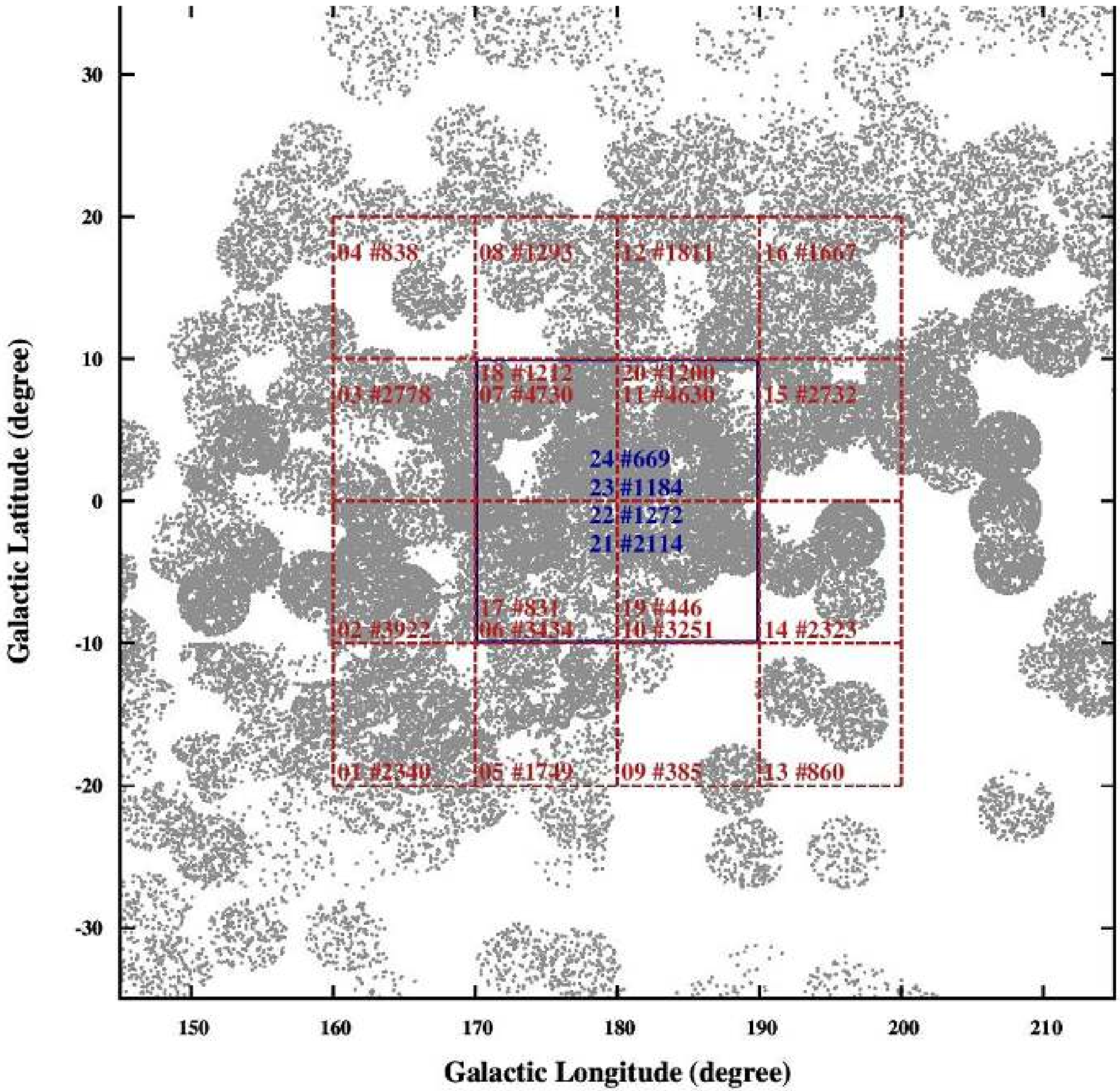

Распределение масс и распределение дисперсий скоростей

In this work, we assume that the Milky Way is axisymmetrical with a gas disc, two stellar discs, and a spheroidal halo and bulge. The density of discs is written as (Dehnen & Binney 1998)

$$\rho_d(R,z) = \frac{\Sigma_d}{2z_d} \exp\left(-\frac{R}{R_d} - \frac{|z|}{z_d} - \frac{R_h}{R}\right) \tag{6}$$

where R_d is the scale length, z_d is the scale height, and Σ_d is the central surface density. The parameter R_h describes a central depression, and is set to be non-zero for the gas disc, and zero for the stellar discs. The spheroidal components have the form

$$\rho_s(R,z) = \frac{\rho_0}{m^\gamma (1+m)^{\beta-\gamma}} \exp\left[-\left(\frac{r_0 m}{r_{cut}}\right)^2\right] \tag{7}$$

where

$$m(R,z) = \sqrt{\left(\frac{R}{r_0}\right)^2 + \left(\frac{z}{q r_0}\right)^2}, \tag{8}$$

and ρ_0 is the central density, r_0 is a scale radius and the parameter q is the axial ratio of the isodensity surfaces. The parameters γ and β are the slopes for the inner and outer density profiles respectively, and r_{cut} is the cutoff radius.

The surface density of a disc is an exponential function

$$\Sigma(L_z) = \Sigma_0 \exp\left(-\frac{R_c}{R_d}\right), \tag{10}$$

where radius R_c is derived by assuming a circular orbit with angular momentum L_z. Given the radius of the Solar circle R_0, the vertical and radial velocity dispersions are controlled by the scale parameter R_σ

$$\sigma_r = \sigma_{r0} \exp\left(\frac{R_0 - R_c}{R_\sigma}\right), \sigma_z = \sigma_{z0} \exp\left(\frac{R_0 - R_c}{R_\sigma}\right). \tag{11}$$

The distribution function of a single disc is controlled by 4 parameters σ_{r0}, σ_{z0}, R_d, and R_σ. The L_0 truncation scale parameter is fixed at the Torus Mapper value of 9780 kpc km s^{-1}(Binney & McMillan 2016). An extra parameter is needed to adjust the *ratio* of the thick to thin discs. In total we have 9 free parameters to control the DF of our two component stellar disc system.

На расстояниях >2 кпк от нас – расхождение с Бинни

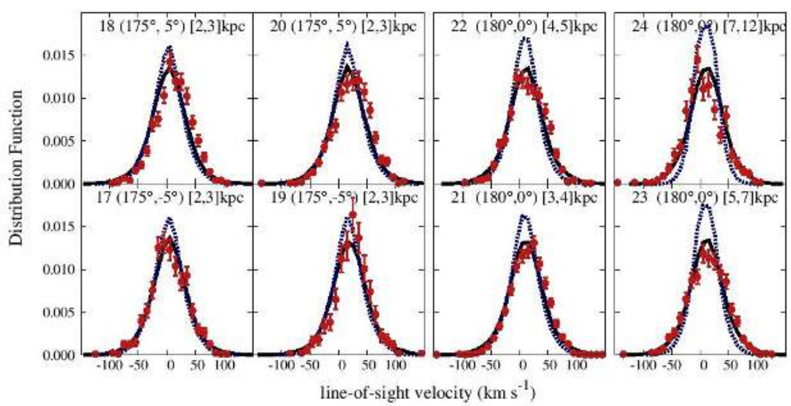

Figure 5. The probability distribution function of the line-of-sight velocity for blocks 17 – 24. The upper left number in each panel is the rank of the block. The corresponding range is listed in Table 1. The black solid and the blue dotted curves represent the predictions from M11b and B12, respectively. The red points denote the data together with the Poisson errors. The longitude and latitude of the centre of each block is indicated together with distance range. Blocks 21 – 24 are 20° × 20°.

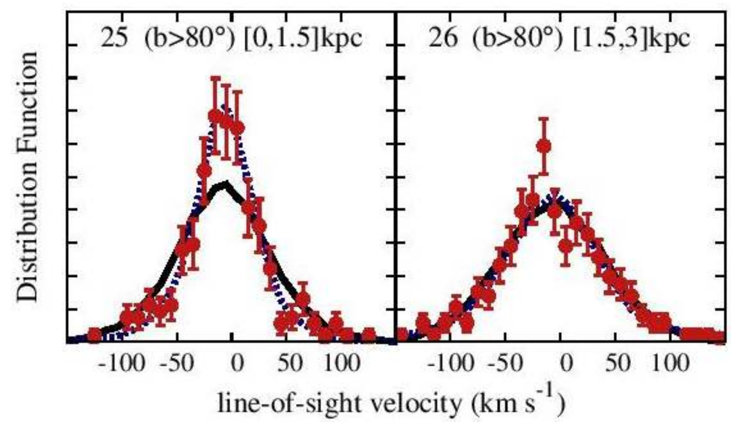

Модели для скоростей

Table 2. χ^2 for the best-fitting parameters of the distribution functions. The fiducial parameters of the DF are labeled by fid. The row of B12 corresponds to the parameters in Binney (2012). The rows labelled from $1-10$ are the models around the second row (fid, M11b) . $\chi^2_{\rm inner}$ is estimated by the first 16 blocks in the Solar neighbourhood, $\chi^2_{\rm middle}$ by (17-20), $\chi^2_{\rm outer}$ by (23, 24), $\chi^2_{\rm Pole}$ by (25, 26) and $\chi^2_{\rm Total}$ is estimated by all of 26 blocks (the blocks are defined in Table 1).

	Thin				Thick				ratio	$\chi^2/d.o.f$				
	(σ_{r0}	σ_{z0}	R_d	R_σ)	(σ_{r0}	σ_{z0}	R_d	R_σ)		(	anti-centre		Pole	Total)
	km s^{-1}	km s^{-1}	kpc	kpc	km s^{-1}	km s^{-1}	kpc	kpc		inner	middle	outer		
B12	40.1	25.6	2.58	8.93	25.8	45.0	2.11	4.04	0.772	3.01	4.28	32.1	1.13	4.50
fid	29.0	42.9	2.41	10.8	50.6	79.3	4.07	19.3	0.67	2.27	2.53	2.38	1.85	2.08
1	26.1	42.9	2.41	10.8	45.5	79.3	4.07	19.3	0.67	2.67	3.54	4.85	2.26	2.61
2	31.9	42.9	2.41	10.8	55.7	79.3	4.07	19.3	0.67	3.35	2.42	5.04	3.77	2.94
3	29.0	38.6	2.41	10.8	50.6	71.4	4.07	19.3	0.67	2.37	2.42	6.18	3.43	2.38
4	29.0	47.2	2.41	10.8	50.6	87.2	4.07	19.3	0.67	2.32	2.50	5.36	2.17	2.25
5	29.0	42.9	2.17	10.8	50.6	79.3	3.66	19.3	0.67	2.52	2.56	3.62	3.64	2.37
6	29.0	42.9	2.65	10.8	50.6	79.3	4.48	19.3	0.67	2.39	2.89	2.91	2.58	2.26
7	29.0	42.9	2.41	9.72	50.6	79.3	4.07	17.4	0.67	2.21	2.88	2.81	2.50	2.15
8	29.0	42.9	2.41	11.9	50.6	79.3	4.07	21.2	0.67	2.47	2.82	4.34	3.34	2.39
9	29.0	42.9	2.41	10.8	50.6	79.3	4.07	19.3	0.60	2.27	2.81	4.16	3.43	2.28
10	29.0	42.9	2.41	10.8	50.6	79.3	4.07	19.3	0.74	2.39	2.37	5.96	2.42	2.32

Модели для плотностей

Table 3. The reduced χ^2 for different mass models. The main parameters of discs, bulge and dark halo are listed in the table. G1 and G2 correspond to the two groups with differing solar position and motions. The best-fitting model is M11b in Group 2. The notation of different mass models is described in Sec. 4.

	Thin		Thick		Gas		bulge			halo			$\chi^2/d.o.f$	
	(Σ_0 $M_\odot/kpc^2$	R_d) kpc	(Σ_0 $M_\odot/kpc^2$	R_d) kpc	(Σ_0 $M_\odot/kpc^3$	R_d) kpc	(ρ_0 $M_\odot/kpc^3$	q	r_0) kpc	(ρ_0 $M_\odot/kpc^3$	q	r_0)	G1	G2
P14	5.71e8	2.68	2.51e8	2.68	9.45e7	5.36	9.49e10	0.5	0.075	1.81e7	1	14.4	4.32	2.59
B12I	1.02e9	2.4	1.14e6	2.4	7.30e7	4.8	1.26e9	0.8	1.09	7.56e8	0.6	1	2.53	2.88
B12II	7.68e8	2.64	2.01e8	2.97	1.16e8	5.28	9.49e10	0.5	0.075	1.32e7	1	16.5	4.27	2.54
M11c	7.53e8	3.0	1.82e8	3.5	-	-	9.41e10	0.5	0.075	1.25e7	1	17	4.36	2.29
M11b	8.17e8	2.9	2.09e8	3.31	-	-	9.56e10	0.5	0.075	8.46e6	1	20.2	3.73	2.08
BT08	1.18e8	2.0	1.66e9	2.0	1.32e8	4.0	7.11e8	0.8	3.83	4.27e8	0.6	1	2.80	2.37

Astro-ph: 1705.00637

A combined photometric and kinematic recipe for evaluating the nature of bulges using the CALIFA sample

J. Neumann[1,2], L. Wisotzki[1], O.S. Choudhury[1], D.A. Gadotti[2], C.J. Walcher[1], J. Bland-Hawthorn[3], R. García-Benito[4], R.M. González Delgado[4], B. Husemann[5], R.A. Marino[6], I. Márquez[4], S.F. Sánchez[7], B. Ziegler[8], and CALIFA collaboration

[1] Leibniz-Institut für Astrophysik Potsdam (AIP), An der Sternwarte 16, D-14480 Potsdam, Germany
[2] European Southern Observatory, Alonso de Córdova 3107, Casilla 19001, Santiago, Chile
[3] Sydney Institute for Astronomy, School of Physics A28, University of Sydney, NSW 2006, Australia
[4] Instituto de Astrofísica de Andalucía (IAA/CSIC), Glorieta de la Astronomía s/n Aptdo. 3004, E-18080 Granada, Spain
[5] Max-Planck-Institut für Astronomie, Königstuhl 17, D-69117 Heidelberg, Germany
[6] Department of Physics, Institute for Astronomy, ETH Zürich, CH-8093 Zürich, Switzerland
[7] Instituto de Astronomía, Universidad Nacional Autonóma de México, A.P. 70-264, 04510 México, D.F., Mexico
[8] University of Vienna, Department of Astrophysics, Türkenschanzstr 17, 1180 Vienna, Austria

Параметр концентрации от морфологического типа

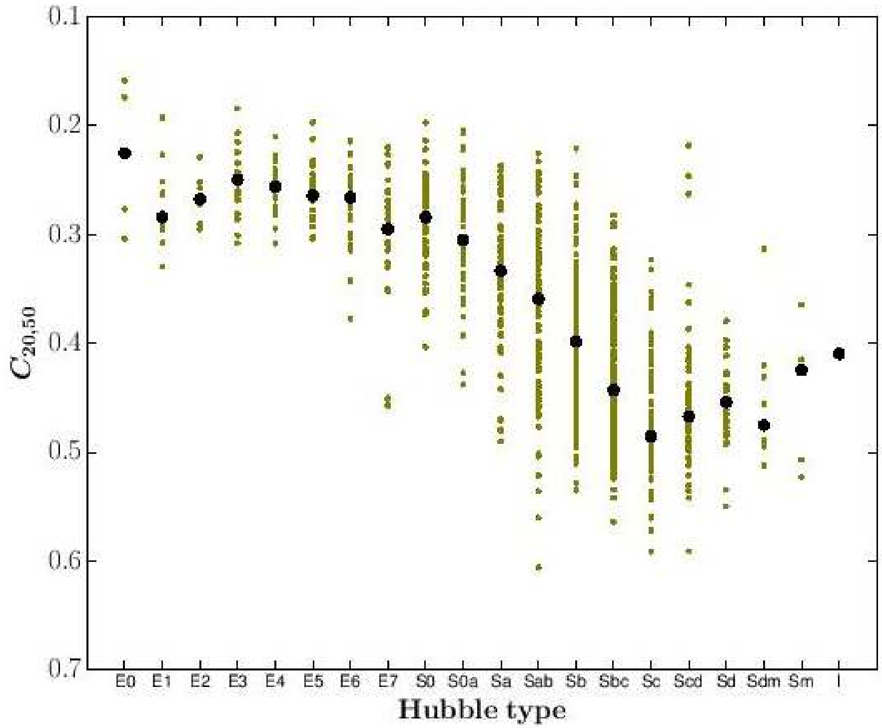

Fig. 6. Relation between $C_{20,50}$ and morphological type for the complete CALIFA mother sample. Median values for each type are marked by big black dots.

Корреляции и критерии

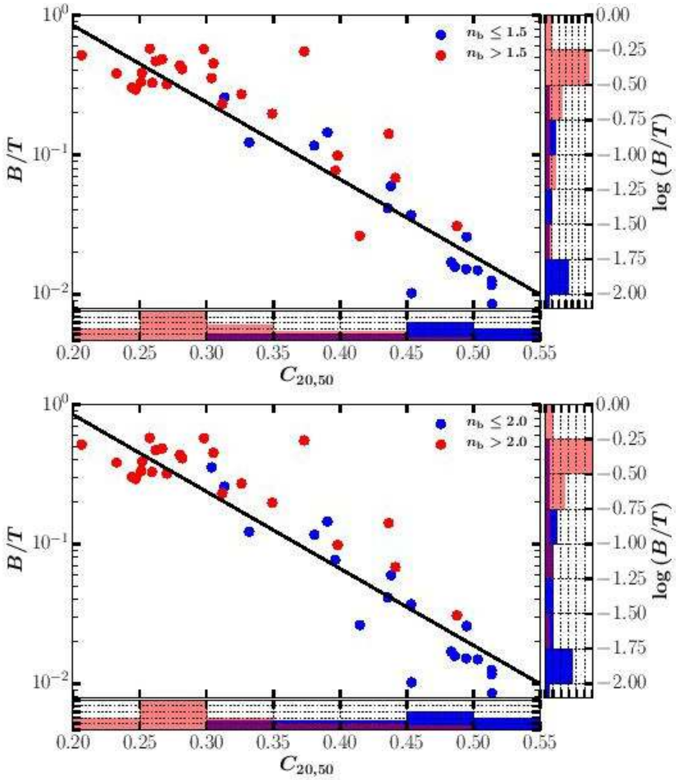

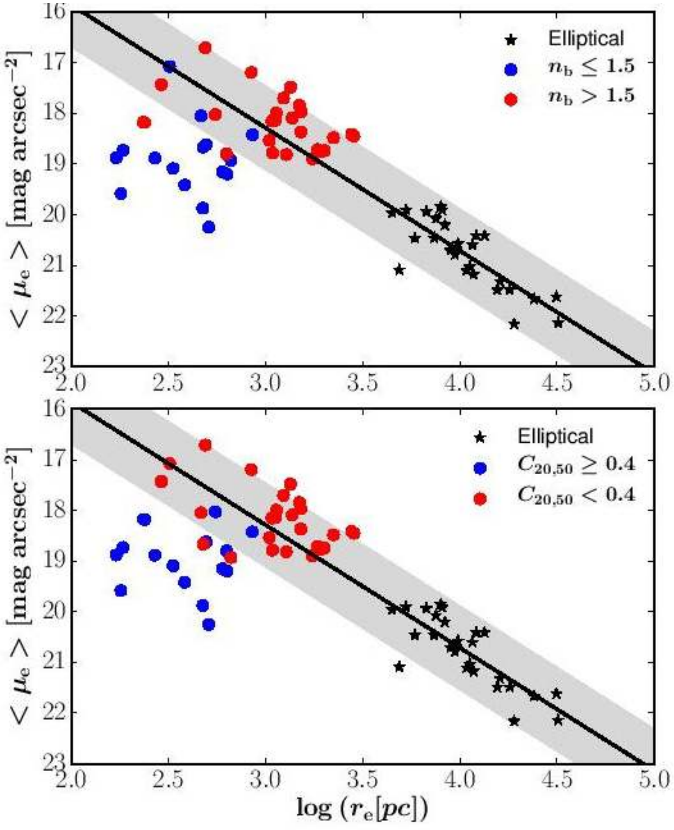

А вот с Фабер-Джексон не сложилось…

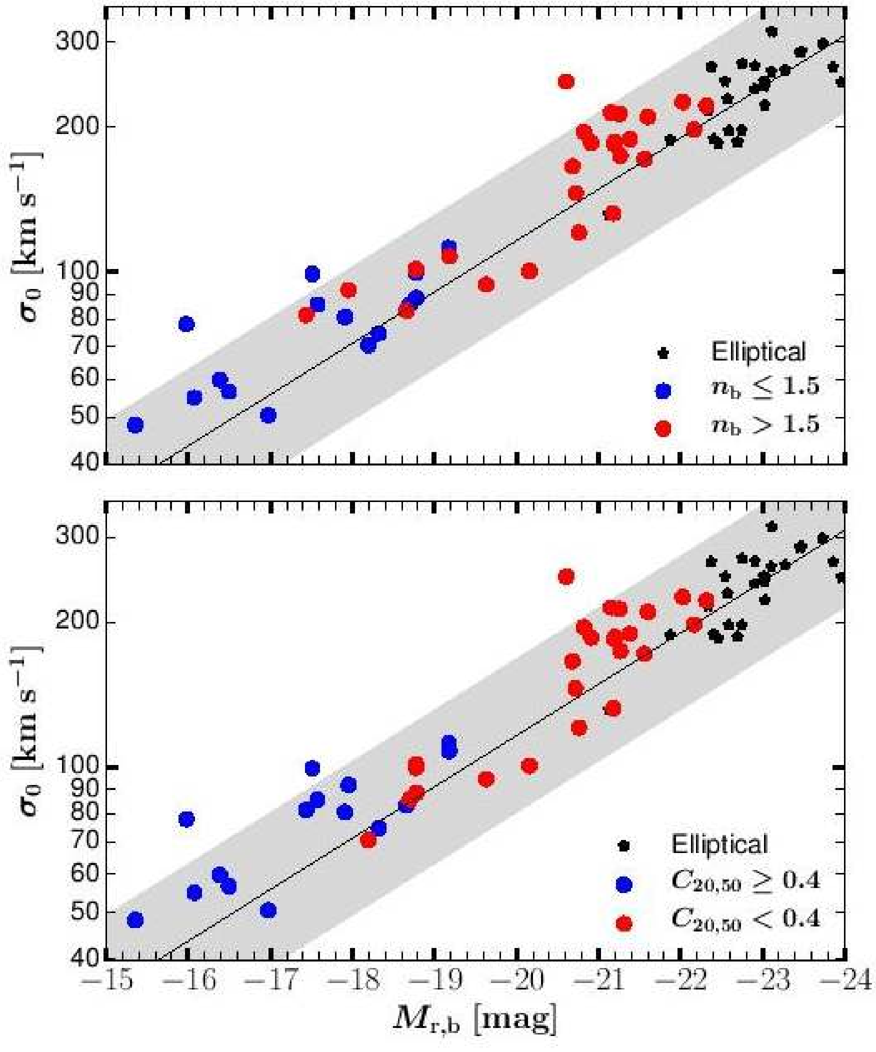

ПРОФИЛЬ дисперсии скоростей – как бы критерий

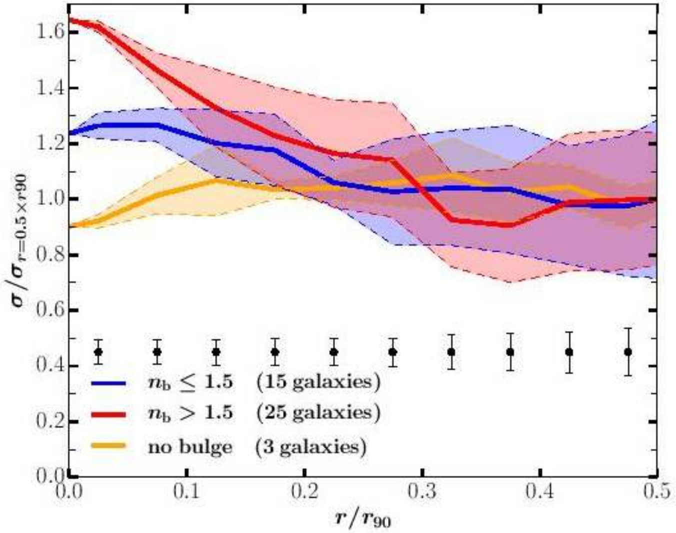

Fig. 11. Average radial velocity dispersion profiles for low-n_b (blue), high-n_b (red) and bulgeless (orange) galaxies. The thick solid lines represent the median profiles and the dashed lines the median absolut deviations. The velocity dispersion is normalised by σ at $r = 0.5\times r_{90}$ and the radial distance is normalised by r_{90} – the radius that encloses 90% of the total light of the galaxy. Error bars at the bottom indicate the median uncertainty for each $0.05 \times r_{90}$ bin.

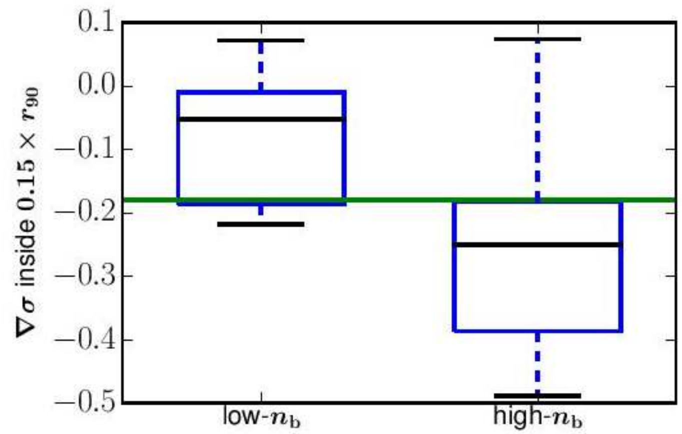

Fig. 13. Boxplot for the velocity dispersion gradient inside $0.15\times r_{90}$ for high- and low-n_b galaxies. The blue box marks the interquartile range of the sample, the black line in the box gives the median value. The top and bottom black line stand for the highest and lowest value, respectively. The thick green line at $\nabla\sigma = -0.18$ gives a good demarcation to separate the subsamples based on the velocity dispersion gradient.

Окончательный список критериев

$$\text{Sérsic index:} \begin{cases} \text{ps} & \text{if} \quad n_\text{b} \le 1.5 \\ \text{cl} & \text{if} \quad n_\text{b} > 1.5 \end{cases}$$

$$\text{Concentration index:} \begin{cases} \text{ps} & \text{if} \quad C_{20,50} \ge 0.4 \\ \text{cl} & \text{if} \quad C_{20,50} < 0.4 \end{cases}$$

$$\text{Velocity dispersion:} \begin{cases} \text{ps} & \text{if} \quad \nabla\sigma \ge -0.18 \\ \text{cl} & \text{if} \quad \nabla\sigma < -0.18 \end{cases}$$

$$\text{Kormendy relation:} \begin{cases} \text{ps} & \text{if the bulge lies below and outside} \\ & \pm 2\sigma \text{ of the relation for elliptical} \\ & \text{galaxies} \\ \text{cl} & \text{if the bulge lies within} \\ & \text{the} \pm 2\sigma \text{ range} \end{cases}$$

Индивидуальная классификация

ID	NED name	B/T	n_b ≤ 1.5	$C_{20,50}$ ≥ 0.4	$\nabla\sigma$ ≥ -0.18	Kormendy rel low-outlier	Classification
(1)	(2)	(3)	(4)	(5)	(6)	(7)	(8)
2	UGC00005	0.01	ps	ps	cl	ps	pseudo
3	NGC7819	0.12	ps	cl	cl	ps	
6	NGC7824	0.38	cl	cl	cl	cl	classical
8	NGC0001	0.41	cl	cl	cl	cl	classical
20	NGC0160	0.29	cl	cl	cl	cl	classical
31	NGC0234	0.04	ps	ps	ps	ps	pseudo
33	NGC0257	0.10	cl	cl	ps	cl	classical
43	IC1683	0.12	ps	cl	cl	cl	classical
45	NGC0496	bulgeless	bulgeless	ps	ps	bulgeless	bulgeless
47	NGC0517	0.55	cl	cl	ps	cl	classical
119	NGC1167	0.23	cl	cl	cl	cl	classical
147	NGC2253	0.08	cl	cl	cl	cl	classical
275	NGC2906	0.14	cl	ps	ps	ps	pseudo
277	NGC2916	0.07	cl	ps	cl	cl	classical
311	NGC3106	0.30	cl	cl	cl	cl	classical
489	NGC4047	0.03	cl	ps	ps	ps	pseudo

Astro-ph: 1705.01115

FURTHER CONSTRAINTS ON VARIATIONS IN THE IMF FROM LMXB POPULATIONS

Mark B. Peacock,[1] Stephen E. Zepf,[1] Arunav Kundu,[2] Thomas J. Maccarone,[3] Bret D. Lehmer,[4] Claudia Maraston,[5] Anthony H. Gonzalez,[6] Rafael T. Eufrasio,[4] and David A. Coulter[7]

[1] *Department of Physics and Astronomy, Michigan State University, East Lansing, MI 48824, USA*

[2] *Eureka Scientific, Inc., 2452 Delmer Street, Suite 100 Oakland, CA 94602, USA*

[3] *Texas Tech University, Lubbock, TX 79409, USA*

[4] *University of Arkansas, 226 Physics Building, 835 West Dickson Street, Fayetteville, AR 72701, USA*

[5] *Institute of Cosmology and Gravitation, Dennis Sciama Building, Burnaby Road, Portsmouth PO1 3FX, UK*

[6] *University of Florida, Gainesville, FL 32611, USA*

[7] *University of California Santa Cruz, Santa Cruz, CA 95064, USA*

Выборка

Name (NGC)	Type[a]	D[b] (Mpc)	ref[b]	σ[c] ($\mathrm{km\,s^{-1}}$)	ref[c]	Mg b[d]	$[Z/H]$[d]	$[\alpha/Fe]$[d]	R_e[e] ($''$)	r_{in}[f] ($''$)	r_{ext}[g] ($''$)	e[g]	L_K[g] ($\times 10^{10}\, L_{K\odot}$)	f_K[g]
1399	E1	20.0	1	280	2	–	–	–	48.6	10	220.2	0.00	25.8	0.78
3115	S0	9.7	4	229	4	–	–	–	34.6	20	249.4	0.61	9.0	0.54
3379	E1	10.6	1	197	1	4.03	-0.11	0.29	40.1	10	191.7	0.15	7.5	0.75
4278	E12	16.1	1	228	1	4.15	-0.06	0.40	31.5	10	155.0	0.07	7.7	0.66
4472	E2	16.7	2	288	1	3.87	-0.22	0.30	94.9	20	313.4	0.19	41.6	0.54
4594	SA	9.0	3	251	3	–	–	–	70.2	22.5*	297.1	0.46	18.0	0.42
4649	E2	16.5	2	308	1	4.23	-0.12	0.36	66.4	20	241.3	0.19	29.6	0.61
4697	E6	11.7	1	180	1	3.30	-0.29	0.26	62.3	10	240.2	0.37	8.3	0.81
7457	SA0	13.2	4	74	1	2.77	-0.19	0.12	36.5	5	155.1	0.45	2.0	0.90

[a] galaxy classifications from de Vaucouleurs et al. (1991)

[b] distances in Mpc derived from surface brightness fluctuation measurements by: (1) Blakeslee et al. (2001); (2) Blakeslee et al. (2009); (3) Jensen et al. (2003); (4) Tonry et al. (2001)

[c] velocity dispersion (σ) from: (1) Cappellari et al. (2012); (2) Saglia et al. (2000); (3) Jardel et al. (2011); (4) van den Bosch (2016) and Emsellem et al. (1999)

[d] Mg b lick index, metallicity and α abundance from McDermid et al. (2015).

[e] The effective radius (R_e), derived using the formulation of Cappellari et al. (2011): the average of the B-band R_e from de Vaucouleurs et al. (1991) and that based on 2MASS LGA data, $R_{e,2MASS} = 1.7 \times median(\mathrm{j\_r\_eff, h\_r\_eff, k\_r\_eff})\sqrt{\mathrm{k\_ba}}$.

[f] The radius defining the central region that is excluded from our analysis *For NGC 4594 we remove an elliptical inner region with semi-minor axis = 22.5$''$and semi-major axis = 168$''$.

Пробуют следующие НФМ…

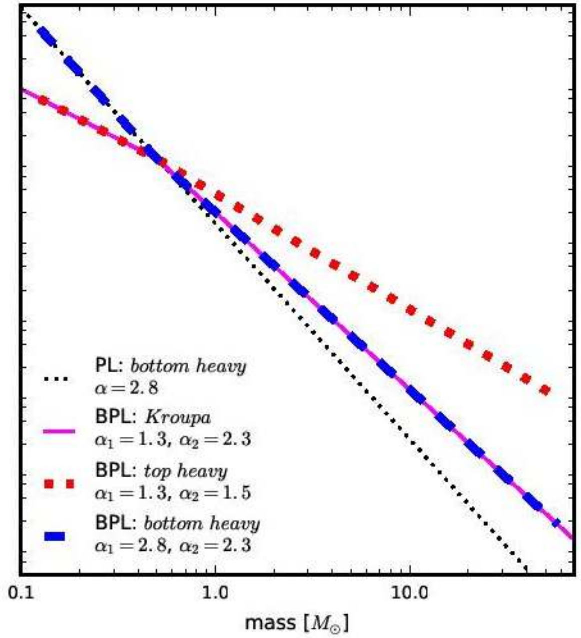

Figure 1. The IMF forms considered in this paper (scaled to have a similar number of stars with $m = 0.5\,M_\odot$). The solid-magenta line shows a Kroupa like IMF. This is similar to that observed in the Milky Way and consists of a broken powerlaw (BPL) with $\alpha_1 = 1.3$ and $\alpha_2 = 2.3$. The dashed-blue line shows a bottom heavy BPL model which is similar Kroupa above $0.5\,M_\odot$, but has a steeper slope at lower stellar mass, with $\alpha_1 = 2.8$. The dotted-red line shows a top heavy

Общая форма НФМ НЕ МЕНЯЕТСЯ

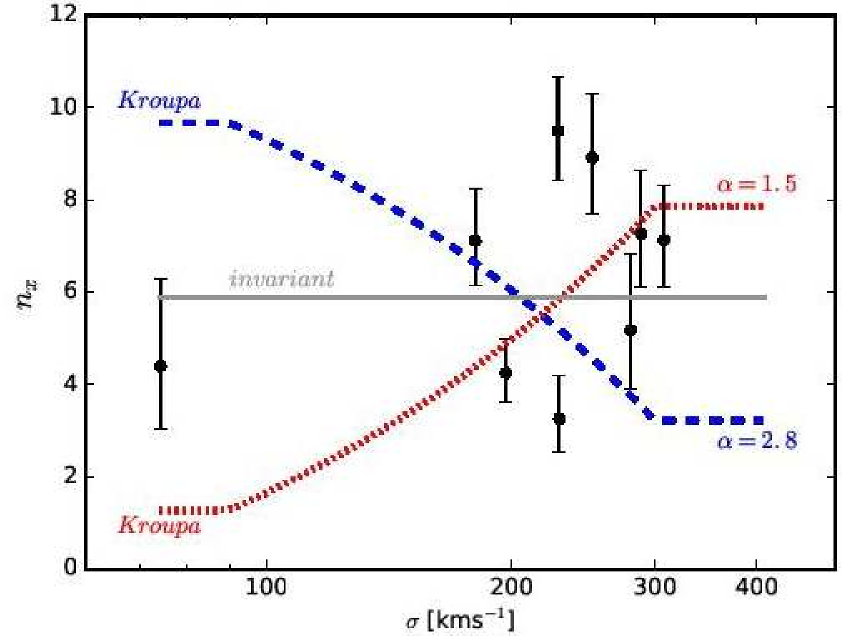

Figure 2. The specific frequency of LMXBs, $n_x = \#LMXBs/10^{10}\ L_{K\odot}$, as a function of velocity dispersion (σ, black points). The lines compare these data to the predictions presented in P14 for an invariant IMF (solid grey line), an IMF which varies from Kroupa at low σ to a single power law with $\alpha = 2.8$ at high σ (dashed blue line), and an IMF which varies from Kroupa at low σ to a single power law with $\alpha = 1.5$ at high σ (dotted red line). The formation efficiency of LMXBs is poorly constrained theoretically. We therefore scale all models to fit the data (and hence predict different n_x at low σ, where all models have a similar IMF).

Ну разве что поправить маломассивный хвост…

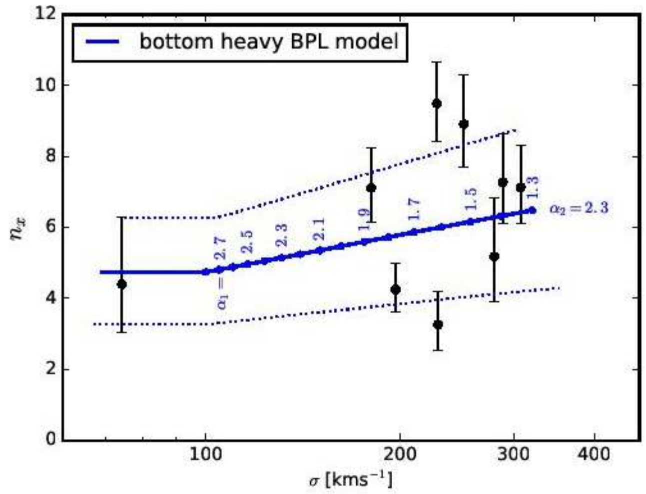

Figure 3. Data as in Figure 2. The solid-blue line shows an increasingly bottom heavy IMF model in which the number of low mass stars ($< 0.5\,M_\odot$) increases systematically with σ, with α_1 increasing from 1.3 to 2.8 (α_2 remains constant at 2.3). The dotted-blue lines are for $\alpha_2 = -2.16$ and -2.48, which are the conservative constraints these data place on variation in the high mass slope.

… или наоборот, массивный хвост…

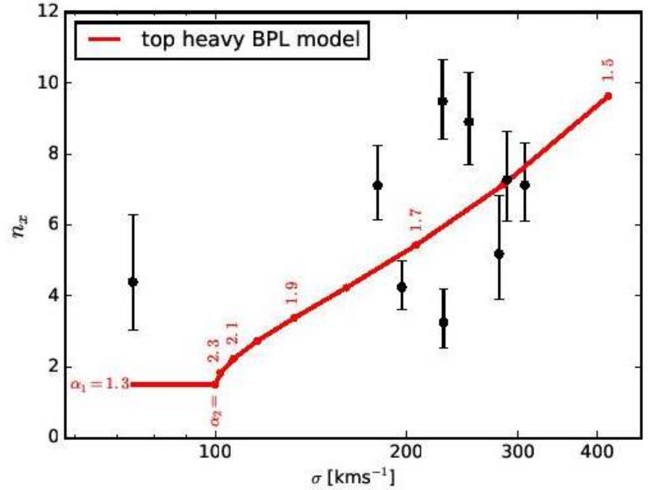

Figure 4. Same as Figure 3, but where the model is based on an increasingly top heavy IMF. In this model, the number of low mass stars ($m < 0.5\,M_\odot$) is constant (with $\alpha_1 = 1.3$) and the number of high mass stars increases with σ (with α_2 varying from 2.3 to 1.5).

Всякие корреляции – объектов мало!

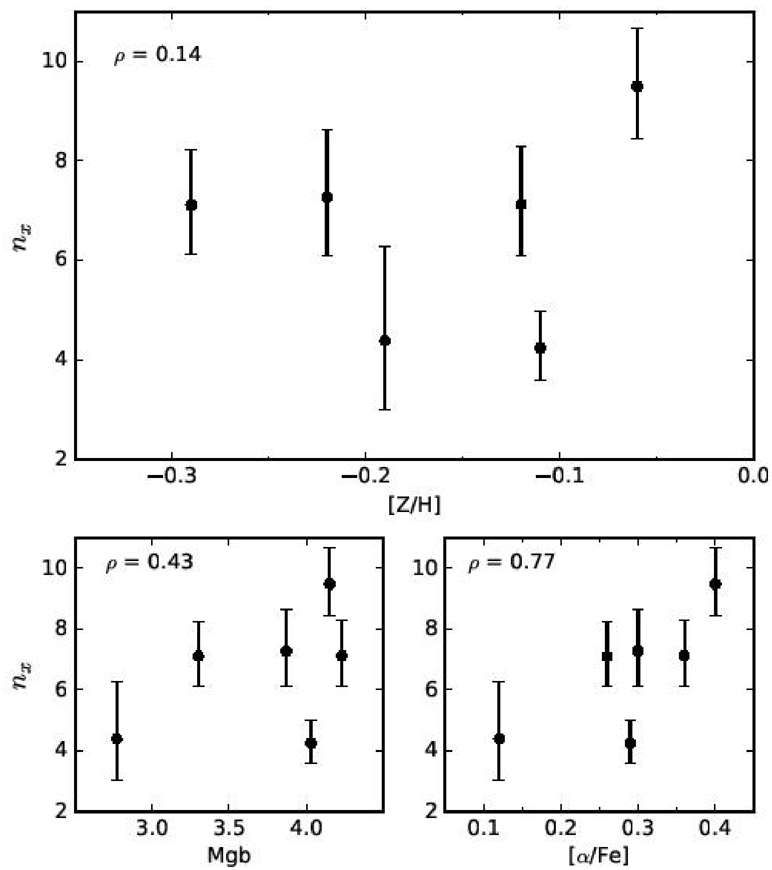

Astro-ph: 1705.01588

LEGACY EXTRAGALACTIC UV SURVEY WITH THE HUBBLE SPACE TELESCOPE.
STELLAR CLUSTER CATALOGUES AND FIRST INSIGHTS INTO CLUSTER FORMATION AND EVOLUTION IN NGC 628[1]

A. Adamo[2], J.E. Ryon[3], M. Messa[2], H. Kim[4], K. Grasha[5], D.O. Cook[44], D. Calzetti[5], J.C. Lee[3, 7], B.C. Whitmore[3], B.G. Elmegreen[8], L. Ubeda[3], L.J. Smith[9], S.N. Bright[3], A. Runnholm[2], J.E. Andrews[10], M. Fumagalli[11], D.A. Gouliermis[12,13], L. Kahre[14], P. Nair[15], D. Thilker[16], R. Walterbos[14], A. Wofford[17], A. Aloisi[3], G. Ashworth[11], T.M. Brown[3], R. Chandar[18], C. Christian [3], M. Cignoni[19,20], G.C. Clayton[21], D.A. Dale[6], S.E. de Mink[22], C. Dobbs[23], D.M. Elmegreen[24], A.S. Evans[25,26], J.S. Gallagher III[27], E.K. Grebel[28], A. Herrero[29,30], D.A. Hunter[31], K.E. Johnson[25], R.C. Kennicutt [32], M.R. Krumholz[33], D. Lennon[34], K. Levay[3], C. Martin[35], A. Nota[9], G. Östlin[2], A. Pellerin[36], J. Prieto[37], M.W. Regan[3], E. Sabbi[3], E. Sacchi[38,39], D. Schaerer[40], D. Schiminovich[41], F. Shabani[28], M. Tosi[39], S.D. Van Dyk[39], E. Zackrisson[43]

Accepted in ApJ, April 30th, 2017

Галактика NGC 628…

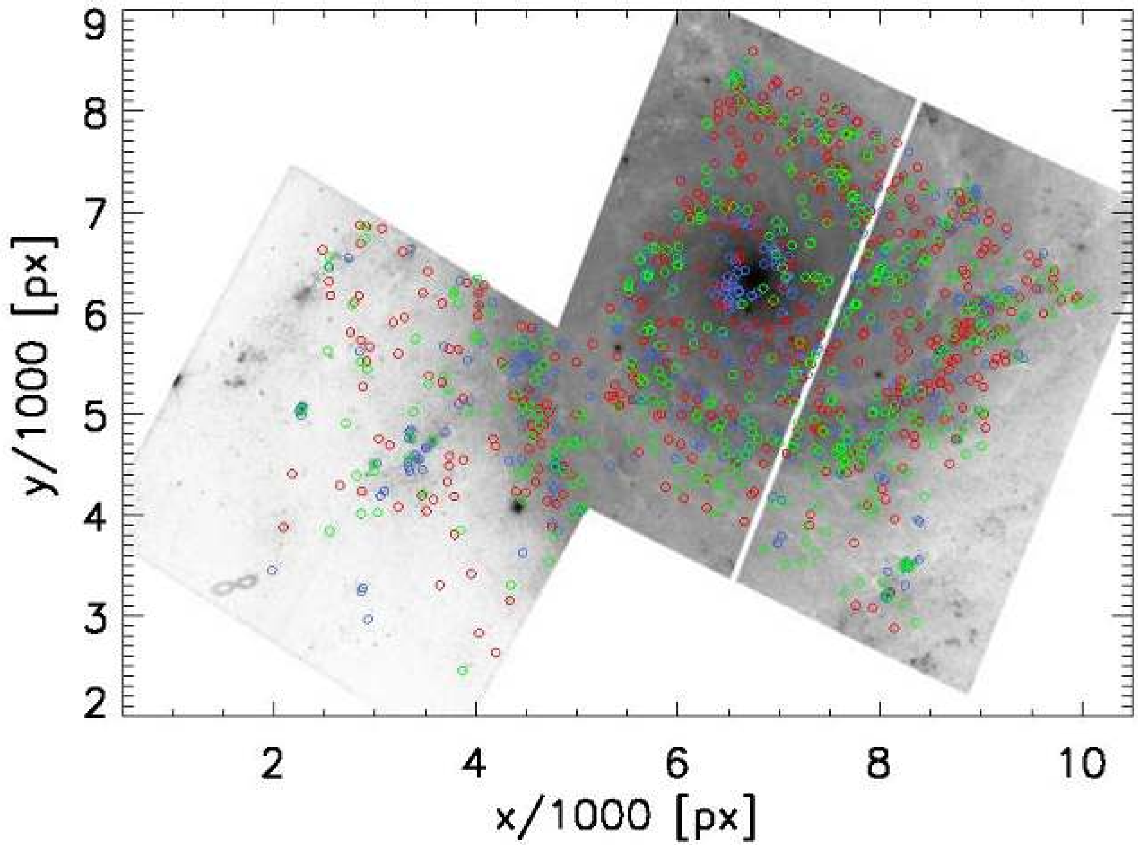

FIG. 1.— A mosaic image of the two F555W pointings of NGC 628, covering the inner part of the galaxy and a portion of the outer disk in the South-East (image rotated with North-up). The circles show the position of class 1 (red), class 2 (green), and class 3 (blue) cluster candidates. See section 2.2.2 for a description of our classification used here. Detected objects are covering the portions of the field of view that are in commune among the imaging taken in the 5 standard LEGUS filters.

… в пяти фильтрах

TABLE 1
THE LEGUS DATASET OF NGC628.

Filters (1)	Program number (2)	PI (3)	exptime sec (4)	ZP(Vega) mag (5)	aver apcor[a] mag (6)	det limits[b] mag (7)	det threshold electron/sec (8)
Inner pointing (NGC628c)							
WFC3/F275W	13364	Calzetti	2481.0	22.632	-0.817± 0.066	23.29	0.009
WFC3/F336W	13364	Calzetti	2361.0	23.484	-0.750 ± 0.060	23.91	0.010
ACS/F435W	10402	Chandar	1358.0	25.784	-0.656 ± 0.034	24.93	0.013
ACS/F555W	10402	Chandar	858.0	25.731	-0.634 ± 0.034	25.05	0.021
ACS/F814W	10402	Chandar	922.0	25.530	-0.751 ± 0.037	24.27	0.030
Outer pointing (NGC628e)							
WFC3/F275W	13364	Calzetti	2361.0	22.632	-0.795 ± 0.097	23.38	0.009
WFC3/F336W	13364	Calzetti	1119.0	23.484	-0.706 ± 0.059	23.48	0.018
ACS/F435W	10402	Chandar	4720.0	25.784	-0.695 ± 0.039	25.26	0.010
WFC3/F555W	13364	Calzetti	965.0	25.816	-0.740 ± 0.038	25.22	0.024
ACS/F814W	10402	Chandar	1560.0	25.530	-0.843 ± 0.050	24.42	0.029

[a] Averaged aperture corrections used to produce the final AV_APCOR cluster catalogues.
[b] The listed values correspond to the 90% completeness limits at the detection thresholds listed in column 8. Completeness limits have been estimated using synthetic clusters with sizes larger than 1 pc. See details about the meaning of the recovered completeness values in the main text.

Классификация

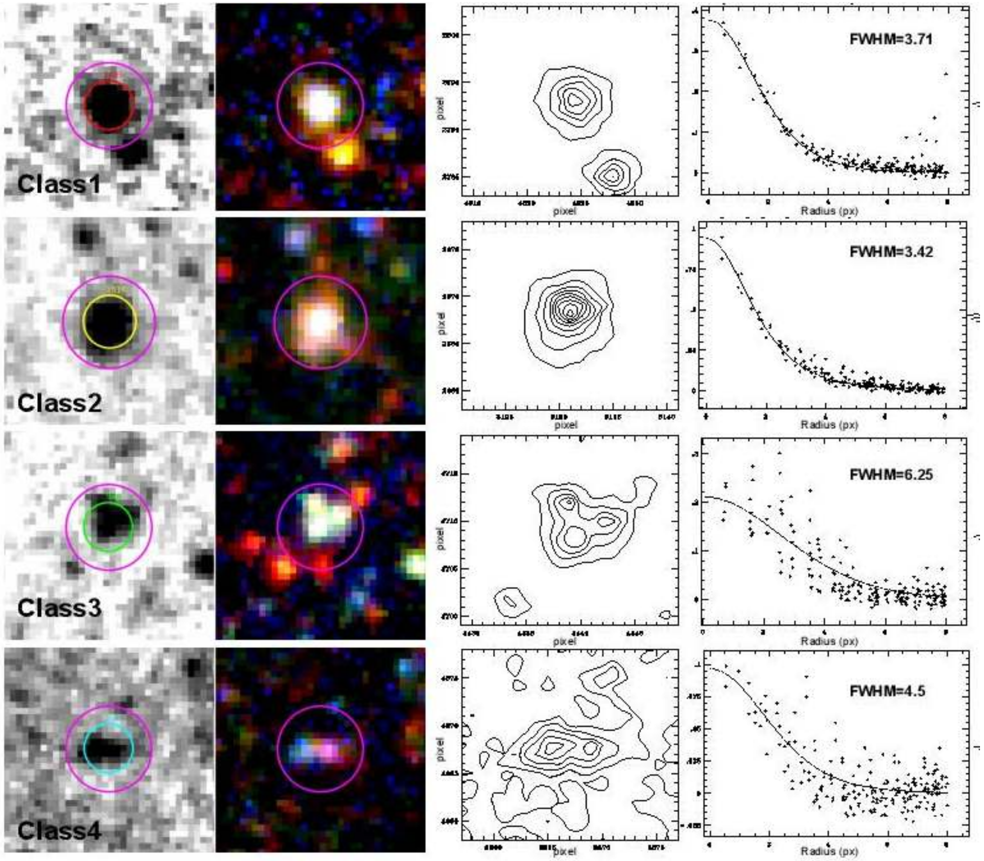

Функции светимости

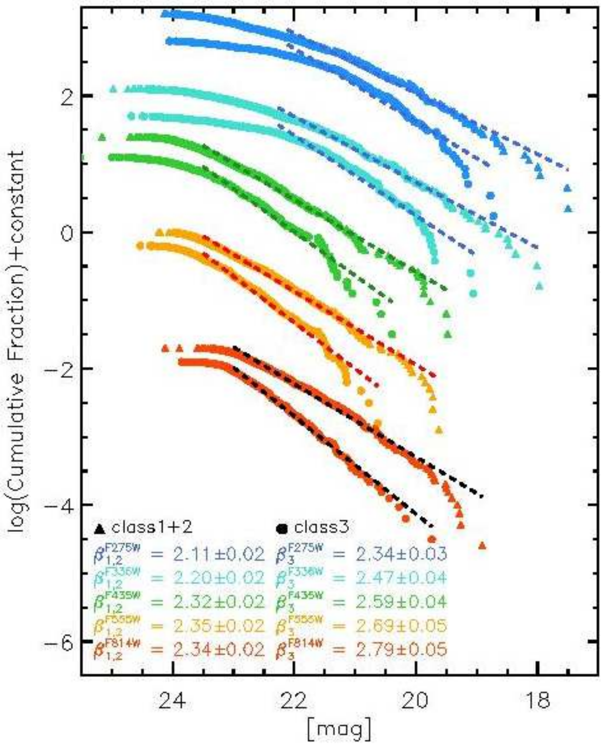

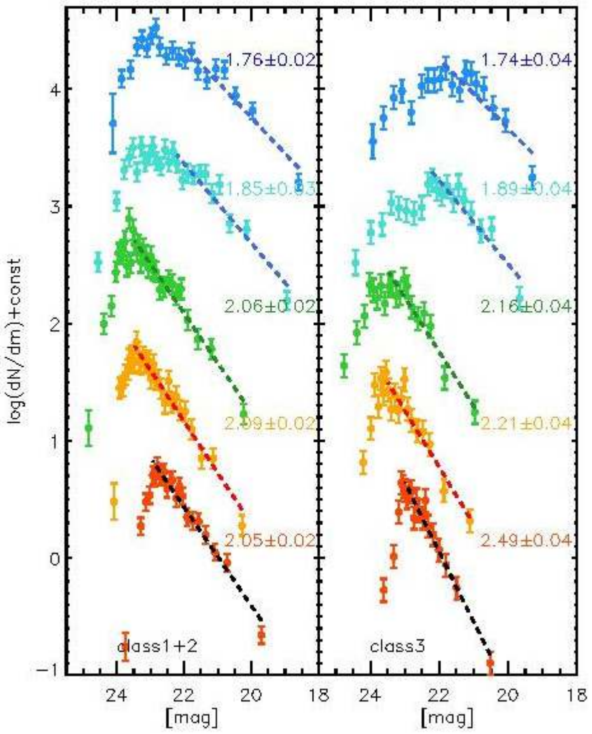

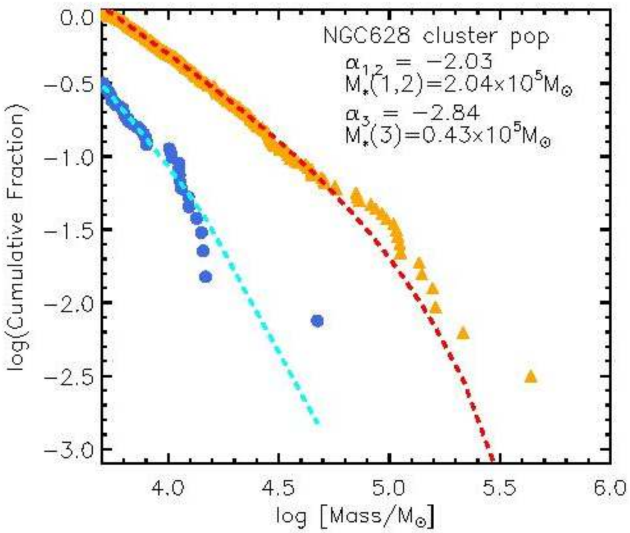

Спекуляции по поводу разрушения

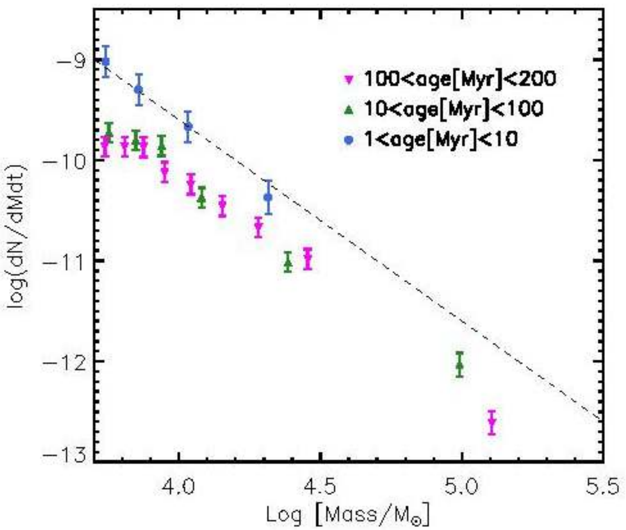

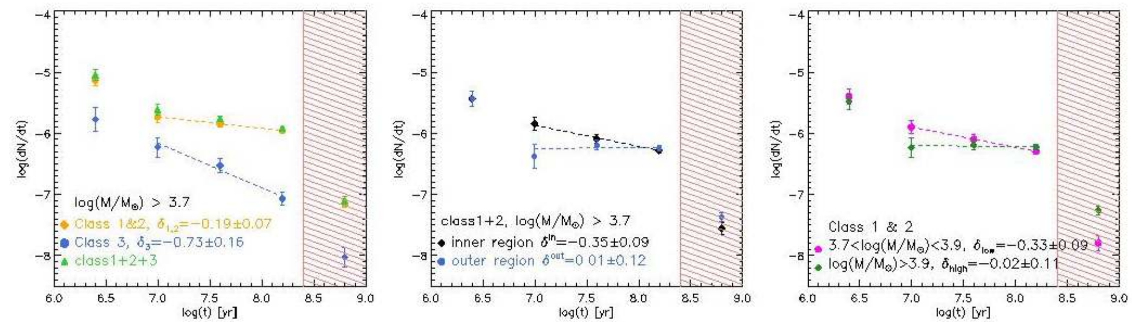

FIG. 19.— Number density of systems more massive than 5000 M$_\odot$ per unit time as a function of age using equally spaced temporal bins (bin size is 0.6 dex). The shadowed areas show the regions of the diagrams that are affected by incompleteness and excluded from the analysis. The fit to each distribution within the age range 10 to 200 Myr is illustrated with a dashed line. The recovered slopes are included in the corresponding insets. The left panel illustrates the change in number density of the whole population (class 1, 2, & 3, green triangles), cluster candidates (class 1 & 2, orange dots), compact associations (class 3, blue diamonds). The central panel shows the number density of clusters as a function of age within an inner and outer region. The two regions contain the same number of clusters with mass above 5000 M$_\odot$. In the left panel we split the sample into low mass ($log(M) \leq 3.9$ M$_\odot$, magenta dots) and high mass ($log(M) > 3.9$ M$_\odot$, green diamonds) clusters. See text to follow the discussion of the results.